RESEARCH ARTICLE | NOVEMBER 10 2025

Orbital inversion mechanisms hidden in strongly correlated radical systems

Jiarui Zeng ; Chang-Chun He ; Shao-Bin Qiu; Yao Yao

Appl. Phys. Lett. 127, 191901 (2025)
https://doi.org/10.1063/5.0292313

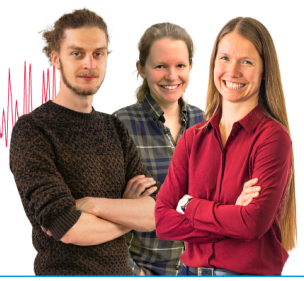

Applied Physics Letters ARTICLE pubs.aip.org/aip/apl

Orbital inversion mechanisms hidden in strongly correlated radical systems

Cite as: Appl. Phys. Lett. **127**, 191901 (2025); doi: 10.1063/5.0292313
Submitted: 22 July 2025 · Accepted: 26 October 2025 ·
Published Online: 10 November 2025

Jiarui Zeng,[1] Chang-Chun He,[2,a)] Shao-Bin Qiu,[3,b)] and Yao Yao[2,4,c)]

AFFILIATIONS

[1]School of Physics and Optoelectronic Engineering, Hainan University, Haikou 570228, China
[2]Department of Physics, South China University of Technology, Guangzhou 510640, China
[3]School of Physics and Electrical Engineering, Jiaying University, Meizhou 514015, China
[4]State Key Laboratory of Luminescent Materials and Devices, South China University of Technology, Guangzhou 510640, China

[a)]Electronic mail: scuthecc@scut.edu.cn
[b)]Electronic mail: qiushaobin@jyu.edu.cn
[c)]Author to whom correspondence should be addressed: yaoyao2016@scut.edu.cn

ABSTRACT

Orbital inversion in organic radical systems is of interest in multiple domains such as spintronics, luminescence, and chemical reactions but requires to comprehend its mechanisms. Here, we reveal an implicit but significant factor for orbital-inverted radical systems. Within the framework of the Hubbard model, the inversion can emerge from nearest-neighbor coulombic repulsion between two electrons having the same spin, which necessitates the fulfillment of charge-transfer properties and chlorine atom substitution. These conditions can also be utilized to explain previous experimental observations where some of radical analogues exhibit orbital inversion while others remain devoid of it. We also discuss the underlying picture and the phase diagram of the orbital inversion, providing a perspective on π-conjugated systems and double inversion. Our results establish a practical approach to nanoscale control of magnetic and optoelectronic properties in radical-based structures.

Organic open-shell neutral radicals serve as platforms for nontrivial physical and chemical phenomena because of their intrinsic unpaired electrons.[1–7] A scenario of current interest is orbital inversion, which emerges from strongly correlated systems,[8–11] where the singly occupied molecular orbital (SOMO) is energetically below the doubly highest occupied molecular orbital (HOMO). The orbital inversion can protect the unpaired electrons from reactions and therefore enhance the stability of the radical systems, complementing conventional strategies for stabilizing radical compounds including kinetic blocking of active reaction sites and delocalization of electrons.[12,13] Therefore, it can be applied to multiple domains such as spintronics,[14] luminescence,[10] and chemical reactions.[15,16]

The coulombic interactions between opposite-spin electrons, exhibited as on-site repulsion, have a central role in orbital inversion. For a strongly correlated closed-shell parent compound, removing one of HOMO electrons deprives it of repulsion and significantly decreases the energy of the other electron, which is able to cause orbital inversion.[17,18] However, the on-site repulsion veils its counterpart, which arises from two electrons holding the same spin. Several types of orbital-inverted compounds have recently been identified,[17,19] and there also exist other inverted configurations such as singly unoccupied molecular orbital-doubly lowest unoccupied molecular orbital (SUMO-LUMO) inversion.[20] These systems may plausibly arise from same-spin repulsion, but direct discussions are missing.

It is the purpose of this Letter to close this gap. By utilizing the Hubbard model to describe our considered compound, we reveal this implicit but significant mechanism that enables orbital inversion. For this model, we describe how local changes in same-spin coulombic interactions are induced by substitution and result in the inversion. The whole process is found to involve avoided crossing that determines critical behavior and phase diagram. We point out even SUMO-LUMO inversion, and a type of double inversion may be achieved within the present framework. Our work paves the way to comprehend orbital-inverted systems and makes the nanoscale manipulation accessible to quantum states and features.

Let us begin by reviewing the orbital inversion through a compound **1**, which contains a biphenylmethyl radical, a π-conjugated moiety, and an anthryl group, as shown in Fig. 1. It is constructed to

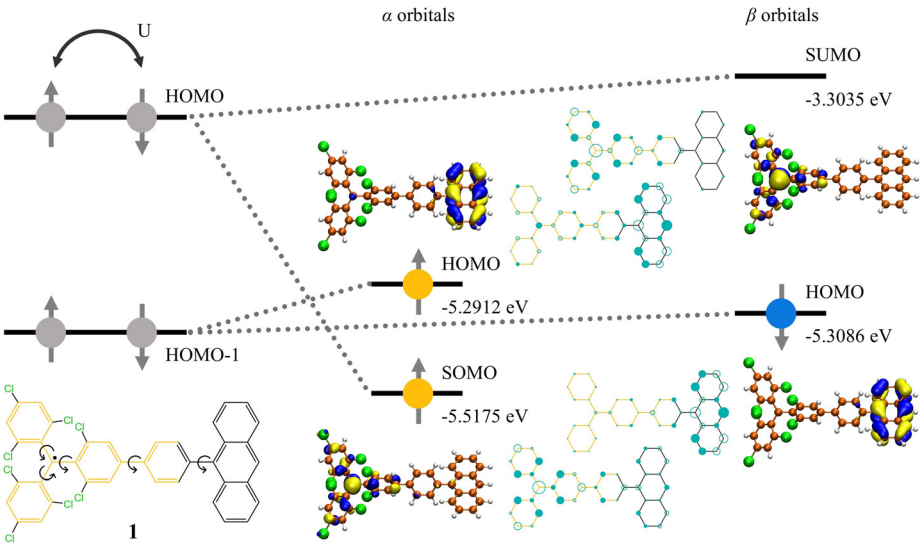

FIG. 1. Sketch of orbital inversion and main results of the compound **1**. For a strongly correlated closed-shell parent compound, when one of the HOMO electrons is removed, the remaining electron experiences a reduction in its energy level, leading to the inverted SOMO. This mechanism is exemplified by **1** (bottom-left panel), of which both the Hubbard model and the DFT results indicate that the SOMO-HOMO inversion occurs. The brown, white, and green spheres represent C, H, and Cl atoms, respectively.

be a polycyclic aromatic hydrocarbon (PAH) based on tris (2,4,6-trichlorophenyl) methyl-phenyl-phenothiazine (TTM-PPTA) that has orbital inversion.[10] The chemical structure of **1** is relatively straightforward to model, facilitating us to discuss its mechanisms. Then, its energies and wavefunction distributions of the three highest occupied orbitals and the lowest unoccupied orbital are calculated through the density functional theory (DFT). Its optimized geometries and UV-Vis spectrum for experimental verification are presented in Table S1 and Fig. S1, respectively. The two occupied orbitals closest to the Fermi level are quasidegenerate, as they exhibit nearly identical level energies and wavefunction distributions on the anthryl group (Fig. 1). Consequently, the two orbitals are designated as the HOMO. Another occupied orbital with lower energy than the HOMO is paired with the lowest unoccupied one rather than other occupied orbitals (Figs. 1 and S2), which corresponds to the SOMO. This exotic phenomenon, compared to conventional radical compounds, indicates the orbital inversion. Previous works have confirmed that the inversion is not an artifact of the computational methodology,[17,19] which is also supported by our results using alternative functionals (Figs. S3 and S4).

In order to comprehend the orbital inversion, we construct the Hubbard model incorporating the on-site repulsion $U = 4$ eV and the nearest-neighbor (NN) repulsion $V_C = 0.55$ eV and $V_{Cl} = 0$. For the compound **1**, the carbon skeleton has an intrinsic V_C, whereas Cl atom substitution reduces the NN repulsion in the influenced moiety, resulting in V_{Cl}. These two types of the NN repulsion are highlighted by black and yellow bonds in Fig. 1, respectively. Through mean-field theory and exact diagonalization, the Hubbard model provides an orbital picture whose wavefunction distributions and level ordering match the DFT results (Figs. 1 and S2). Although the level energies calculated from the Hubbard model differ from the DFT results because we neglect those constant terms of the Hamiltonian, their relative spacings exhibit good agreement (Table S2). Figure S5 supports that the model is robust with respect to V_C and V_{Cl}, as parameter variations hardly alter the SOMO-HOMO inversion. This manifests that the proposed model captures key mechanisms of orbital inversion.

One might be confused about the motivation of introducing the NN repulsion. Most of the PAHs have good π-conjugation, allowing their electronic structures to be accurately described using tight-binding models,[21,22] e.g., graphene.[23] While strong correlation effects need to be considered for some compounds because of their localized features, conventionally only the on-site repulsion is included.[19,24] This treatment resembles transition metal materials, where localized d-orbital electrons necessitate strong correlation corrections for accurate characterization.[25] However, our results show that considering the NN repulsion and distinguishing between V_C and V_{Cl} is crucial for capturing the orbital inversion. Figure 2 presents the four highest occupied α orbitals of the compound **1** obtained from the DFT and the Hubbard models. It can be clearly seen that the model provides a good description even for the HOMO-2 [Figs. 2(a) and 2(b)]. However, if only the on-site repulsion is considered, the Hubbard model not only fails to predict the orbital inversion but also misrepresents the wavefunction distribution of the HOMO-2 [compared to HOMO-1 in Fig. 2(a)].

As aforementioned, the distinction between V_C and V_{Cl} arises from the Cl atom substitution. To understand this, we perform DFT calculations on the compound **1** with its Cl atoms replaced by H atoms (labeled as the compound **2**, optimized geometries are in Table S3). It exhibits nearly identical orbital wavefunction distributions to **1**, except for inversions between the SOMO and HOMO and between the HOMO-1 and HOMO-2 [Figs. 2(a) and 2(e)]. This resemblance manifests that neither Cl nor H atoms contribute significantly to the renormalized π-electrons near the Fermi level. Consequently, they are not treated as occupied sites in the Hubbard model. For the pure PAH **2**, the intrinsic NN repulsion V_C will not impact orbitals near the Fermi level but determines the wavefunction distributions of the deeper orbital. In this context, including V_C yields a more accurate electronic structure [Fig. 2(d)]. Introducing Cl atoms can decrease the NN repulsion of the influenced moiety, which is also supported by Mulliken populations of p-orbital electrons at carbon atoms (Table S4). The populations at the anthryl group hardly change, while they obviously decrease at the biphenylmethyl radical. To determine the moiety with V_{Cl}, we perform parallel computations considering different influenced

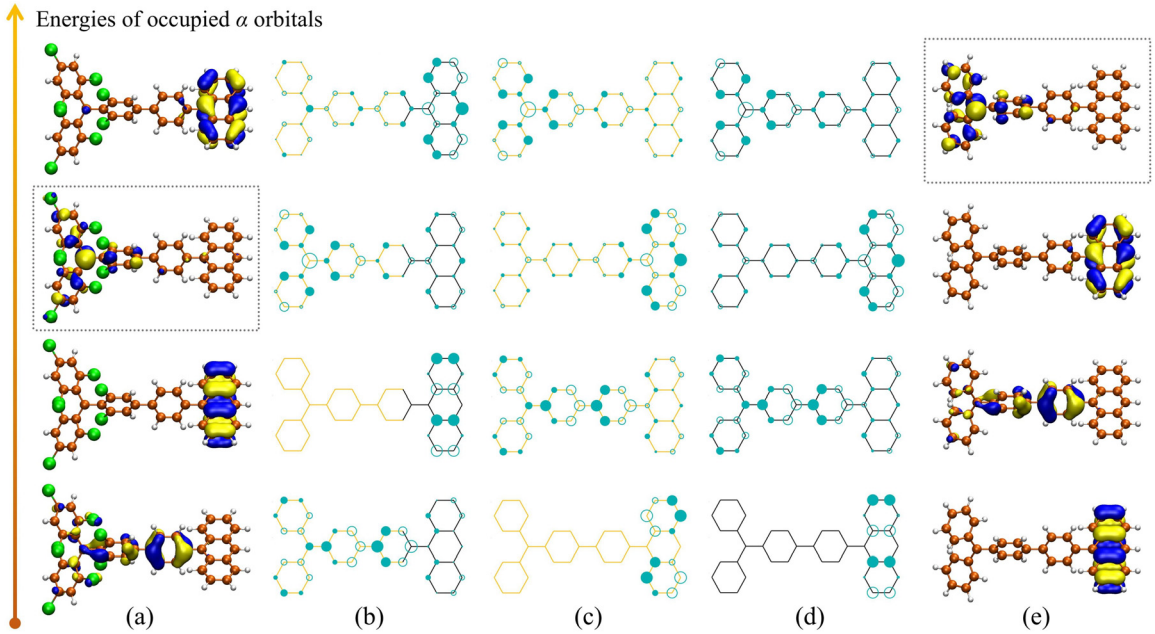

FIG. 2. (a) and (e) Wavefunction distributions of the four highest occupied α orbitals calculated using the DFT, where Cl atoms of **1** are substituted by H atoms in (e). (b)–(d) Wavefunction distributions of the four highest occupied α orbitals calculated using the Hubbard model, where (b) $V_{Cl} = 0$ and $V_C = 0.55$ eV, (c) $V_{Cl} = V_C = 0$, and (d) $V_{Cl} = V_C = 0.55$ eV, respectively. The SOMOs obtained from DFT calculations are framed with gray dotted lines. In panel (a) and (b), orbital inversion occurs as the SOMOs are energetically below the HOMOs.

moiety (Figs. 2 and S6). By comparing their model results with those from DFT calculations, the optimal pattern can be acquired.

Since substitution is able to adjust the NN repulsion, a fundamental question arises: What are the underlying mechanisms and the phase diagram of orbital inversion in strongly correlated systems? Focusing on the compound **1**, we present the level energies of the two highest occupied α (lowest unoccupied β) orbitals with respect to V_{Cl} [Fig. 3(a)]. The yellow solid (dashed) line represents the SOMO (SUMO), while the blue solid (dashed) line refers to the α HOMO (β LUMO). For the pure PAH, there is no orbital inversion at $V_{Cl} = 0.55$ eV. Although the on-site repulsion has decreased the SOMO-HOMO gap, this effect is not sufficient to invert the orbital ordering due to the π-conjugation of the PAH. Nevertheless, based on the charge-transfer properties, one can locally adjust the NN repulsion to control the orbital energies. In **1**, the biphenylmethyl radical and the anthryl group constitute a donor-acceptor structure, resulting in the SOMO and HOMO concentrated on respective groups. Cl atom substitution reduces V_{Cl}, protecting orbitals on the radical and remaining those on the anthryl group influenced by the NN repulsion. Hence, we acquire the decreasing energy of the SOMO and the nearly invariant energy of the HOMO when V_{Cl} decreases. Notably, the system exhibits critical behavior when $V_{Cl} \approx 0.25$ eV, as its SOMO and HOMO hybridize and delocalize over the carbon skeleton [Fig. 3(b)]. This hybridization arises from avoided crossing, at which the energies of the SOMO and HOMO in the diabatic picture converge. Subsequently, their off diagonal coupling (referring to hopping integral) mixes the orbitals and opens a gap in the adiabatic picture.

The hybridization-induced delocalized orbitals may enhance radical stability, similar to that observed in delocalized PAHs. In this sense, identifying real materials at or near the critical point and investigating their properties is an interesting open question. Although this lies beyond the scope of the current paper, we note that the avoided crossing is able to drive phase transitions and alter the ordering of molecular orbitals, offering an alternative stabilization scenario. As V_{Cl} further decreases, the level difference between the SOMO and HOMO will increase in the diabatic picture. Even acquiring molecular orbitals in the adiabatic picture, the SOMO and HOMO remain well-separated against the influences of their off diagonal coupling. Because of the significantly decreasing NN repulsion of the biphenylmethyl radical, the SOMO is energetically lowered below the HOMO, resulting in orbital inversion. The whole process synergistically combines two types of repulsion, charge-transfer properties, and avoided crossing, providing a practical perspective on qualitative experimental design of orbital-inverted compounds.

This synergetical mechanism can answer why TTM has no orbital inversion.[26] Because the TTM does not have charge-transfer properties, its orbitals are distributed on the same moiety and influenced by the same NN repulsion. Accordingly, the orbitals are together energetically shifted, resulting in a conventional electronic structure. Furthermore, based on the proposed mechanism, a qualitative design approach for orbital-inverted systems can also be derived. We show a compound **3** having SOMO-HOMO inversion at the DFT level by substituting Cl atoms with another radical compound **4** (Fig. S7). Their optimized geometries are listed in Tables S5 and S6. The compound **3** has a similar structure to **1**, which might be synthesized using analogous methods. Through measurements of electrochemical potential and electron paramagnetic resonance, the orbital inversion could be validated.[20]

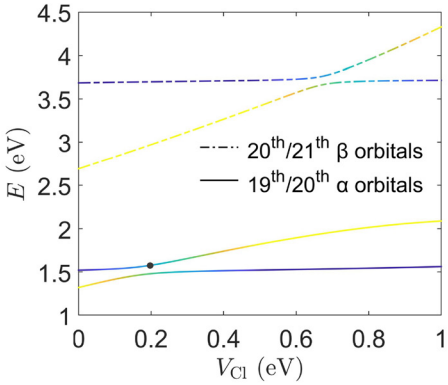

(a) Orbital energies with respect to V_{Cl} at U = 4 eV.

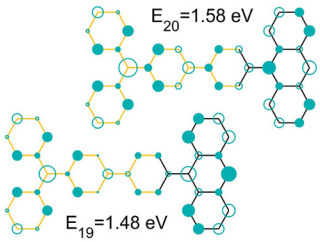

(b) Wavefunction distributions of the two highest occupied α orbitals at U = 4 eV and V_{Cl} = 0.2 eV.

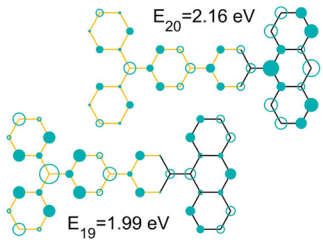

(d) Wavefunction distributions of the two highest occupied α orbitals at U = 5.2 eV and V_{Cl} = 0.55 eV.

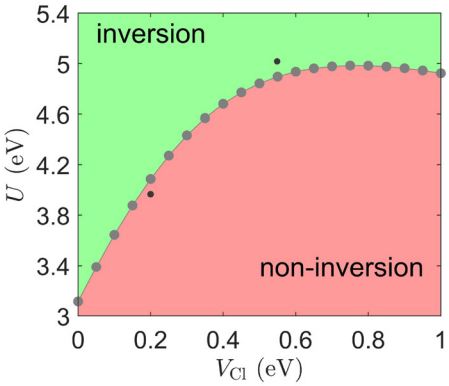

(c) Phase diagram of orbital inversion with respect to U and V_{Cl}.

FIG. 3. Influences of the NN repulsion V_{Cl} and on-site repulsion U on orbital inversion.

It is interesting that varying V_{Cl} not only enables inversion between the SOMO and HOMO but can also induce the SUMO-LUMO inversion. As presented in Fig. 3(a), increasing V_{Cl} elevates the energy of the SUMO while remaining the LUMO hardly influenced. This result is reasonable because the SUMO is on the biphenylmethyl radical. When $V_{Cl} \approx 0.68$ eV, these two orbitals approach quasidegeneracy, and the system exhibits the avoided crossing. Subsequently, the SUMO and LUMO separate again and achieve inversion. This type of orbital inversion has been observed in previous experiments,[20] in which the synthesized molecules are structurally analogous to the compound **1**. Therefore, we believe that it is practical to understand the experimental results by our proposed perspective. To validate the inversion mechanism, a possible approach is to gradually vary the composition of synthesized compounds from pure polycyclic aromatic hydrocarbons to substituted derivatives. The reduction potentials and the radical characteristics can be measured electrochemically to determine the orbital energies.[20] Based on this, the optimal NN repulsion that best matches the experimental results can be inferred. If the present model captures the mechanism of SUMO-LUMO inversion, the acquired NN repulsion would undergo continuous changes as the compounds are substituted. However, the reported compounds are not fully based on a carbon skeleton and, thus, require remodeling, such as using the Pariser-Parr-Pople model,[27–30] which is beyond our current scope in this work. Nevertheless, our results suggest that finding strategies to enhance the NN repulsion is a possible direction to achieve the SUMO-LUMO inversion.

The critical point of the avoided crossing can be identified as the minimum gap between two relevant levels, defining the phase transition boundary for orbital inversion. By further varying the on-site repulsion U, the corresponding phase diagram can be acquired [Fig. 3(c)]. It is found that orbital inversion does not occur at small U, indicating that the on-site repulsion is the central factor for driving the inversion. This case corresponds to delocalized PAHs, which implies that their radical products might be trivial. Typically, 3.5 eV $\lesssim U \lesssim$ 4 eV for those carbon skeletons with localized features,[19,24] but there is also no orbital inversion in pure PAHs without substitution. Nevertheless, as V_{Cl} decreases toward zero, the system undergoes a phase transition where the orbital inversion occurs.

The on-site repulsion again manifests its dominant role for $U \gtrsim 4.98$ eV, where orbital inversion always occurs for all considered values of V_{Cl}. This inversion also involves the avoided crossing and exhibits the hybridization of the SOMO and HOMO [Fig. 3(d)]. Interestingly, both the SOMO-HOMO and the SUMO-LUMO inversions are enabled within the parameter regime of large U (Fig. S8). This provides a possible strategy to achieve double inversion, i.e., the SOMO-HOMO and the SUMO-LUMO inversions occur simultaneously. It should be mentioned that for larger on-site repulsion $U \gtrsim 5.4$ eV, the mean-field theory will be invalid and needs density matrix renormalization group or quantum Monte Carlo methods for correct descriptions. This situation might exist in other types of chemical compounds, which is a possible investigating direction.

Although the large U is unphysical for PAHs, an alternative method can achieve equivalent effects by twisting the compounds. Taking the compound **2** as an example, we artificially maintain the dihedral angles within the biphenylmethyl radical and between the radical and the 6-membered ring at the same value θ, to discuss torsion-induced inversion. It can be clearly seen that for $\theta = 70°$, the SOMO (SUMO) is energetically below (above) the HOMO (LUMO), indicating that the double orbital inversion occurs [Fig. 4(a)]. This result is similar to that of large $U = 5.2$ eV, whereas no inversion occurs at $\theta = 0°$ and $U = 4$ eV (Fig. S9), which manifests that the change of the dihedral angles is the key factor. Spin polarization further reveals that the torsion reduces the π-conjugation and enhances the system localization, facilitating the on-site repulsion and, thus, inducing the double inversion [Figs. 4(b) and 4(c)]. To discuss the structural energetics and synthetic feasibility, we perform DFT structural optimizations with fixed θ, which are coarsely adjusted in 10° increments. The results indicate that although the required θ is larger than that predicted by the Hubbard model, the double inversion is observed at 90° (Fig. S10). DFT calculations show that the total energy of the twisted conformation with $\theta = 90°$ is approximately 1 eV higher than that of the untwisted one. Although such an energy difference makes it challenging to be thermally accessible, it may be kinetically accessible as a metastable state.

In conclusions, we have investigated a mechanism that drives orbital inversion within the framework of the Hubbard model, whose basic idea is to adjust the NN repulsion through Cl atom substitution. Conventionally, this chemical modification is used to change orbital energies or block active reaction sites in radical systems, but our results show that it can also enable control over strongly correlated systems. In addition, we found that a type of double inversion can be achieved by enhancing the on-site repulsion. Although the on-site repulsion depends on the atomic species of the occupied sites and is not easy to adjust, one can alternatively twist the radical compounds to reduce the degree of the π-conjugation.

Our efforts also established a practical perspective on other chemical compounds, which have been synthesized in previous experiments and *a priori* approaches to design orbital-inverted materials combined with nontrivial magnetic and photoelectronic properties.[31–35] Despite inherently limited to PAHs, the present theoretical framework may still offer valuable qualitative insights for interpreting experimental measurements of other types of chemical compounds. Moreover, it is also a possible direction to extend the current model for compounds containing heteroatoms (for example, B and N atoms) and systematically investigate the influences of different substitution patterns and functional groups. Extending this theoretical approach to quantitatively capture broader chemical systems is also our future scope.

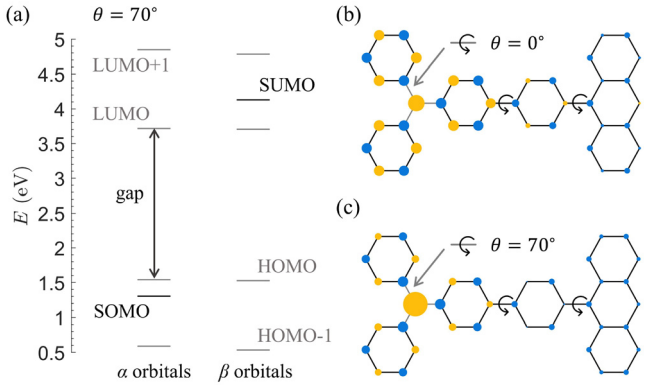

FIG. 4. (a) Level spectrum of the compound **2** with a torsion angle $\theta = 70°$, in which both SOMO-HOMO and SUMO-LUMO inversions occur. (b) and (c) Spin polarization of **2** with $\theta = 0°$ and $\theta = 70°$, respectively. The three dihedral angles labeled with gray lines are maintained at the same torsion value θ. All the results are obtained from the Hubbard model with $U = 4$ eV and $V_C = V_{Cl} = 0.55$ eV.

Methods. Organic radical systems can be effectively modeled using the tight-binding approximation, in which the nearest-neighbor hopping integral corresponds to individual chemical bonds.[36,37] For strongly correlated systems, we further introduce the on-site and the nearest-neighbor repulsive interactions, thereby establishing the Hubbard model:[38–40]

$$H = -\sum_{j\neq i,s} t_{ji} c_{js}^{\dagger} c_{is} + \sum_{i} U_{ji} n_{i\uparrow} n_{i\downarrow} + \sum_{j\neq i,s} V_{ji} n_{js} n_{is}, \tag{1}$$

where j and i refer to occupied carbon sites, $s = \{\uparrow, \downarrow\}$ indicates spin-1/2 up or down, c_{is} ($c_{is}^{\dagger}$) denotes a fermionic annihilation (creation) operator, and $n_{is} = c_{is}^{\dagger} c_{is}$. $t_{ji} = t = -2.7$ eV and $U_{ji} = U = 4$ eV are the hopping integral between the nearest-neighbor sites and the on-site repulsion, respectively, which are adopted as a constant independent of sites unless specified otherwise.[19] The nearest-neighbor repulsion is adopted as $V_{ji} = V_C = 0.55$ eV for pure PAHs.

For the compound **1**, dihedral angles θ between planar moieties are nonzero, which are illustrated in Fig. 1. They result in the sinusoidally decreasing hopping integral as $t_{ji} = t \cos\theta$.[41] According to DFT calculations, both two dihedral angles in the biphenylmethyl radical are 48.3°. The other dihedral angles are 47.0° (biphenylmethyl group/6-membered ring), 34.8° (inter-ring), and 70.2° (6-membered ring/anthryl group). Introducing Cl atoms may locally modify V_{ji}, sketched by yellow bonds in **1** of Fig. 1. In this case, the relevant V_{ji} is modified to be $V_{Cl} = 0$.

When $U \lesssim 2t$, the Hubbard model can be safely approximated utilizing the mean-field theory, i.e., $n_{js} n_{is'} = \langle n_{js}\rangle n_{is'} + n_{js}\langle n_{is'}\rangle - \langle n_{js}\rangle\langle n_{is'}\rangle$.[24,42] Then, we neglect the constant term $\langle n_{js}\rangle\langle n_{is'}\rangle$ and diagonalize and iterate H, acquiring the ν-th orbital wavefunction $\psi_{\nu s}$ for further discussions.[43] Spin polarization can be obtained using $\rho = \rho_{\uparrow} - \rho_{\downarrow}$, where $\rho_s = \sum_{\nu} |\psi_{\nu s}|^2$ is calculated by taking all the occupied orbitals into account.

DFT calculations are conducted with the Gaussian 16 program package.[44] We optimize molecular geometries and calculate orbital wavefunctions and energies at the unrestricted B3LYP/6-31G(d,p) level with the DFT-D3 dispersion correction.[45–48] Main results of orbital inversion are confirmed at the unrestricted M06-2X/TZVP and HSE06/6-311G(d,p) levels.[49,50] All the DFT calculations are at a neutral state and in vacuum and carried out at ultrafine grid integration. Multiwfn package is applied to calculate orbital distributions, Mulliken populations, and UV-Vis spectra.[51,52] Visual Molecular Dynamics package is used to draw molecular structures and isosurface maps.[53]

See the supplementary material for UV-Vis spectroscopy, wavefunction distributions and level energies of the six molecular orbitals of the compound **1**, confirmation of the independence from the computational functionals, validation of the robustness of the model parameters, determination of the influenced moiety by the Cl atom

substitution, a predicted orbital-inverted compound, wavefunction distributions and level spectrum induced by the torsion effects, and optimized geometries of compounds.

This work was supported by the Start-up Research Foundation of Hainan University (Grant No. XJ2500000571), the National Natural Science Foundation of China (Grant Nos. 12374107, 12564063, and 12504268), the Guangdong Basic and Applied Basic Research Foundation (Grant No. 2023A1515110894), and the Fundamental Research Funds for the Central Universities (Grant No. 2025ZYGXZR039).

AUTHOR DECLARATIONS

Conflict of Interest

The authors have no conflicts to disclose.

Author Contributions

Jiarui Zeng: Data curation (equal); Formal analysis (equal); Visualization (equal); Writing – original draft (equal). **Chang-Chun He:** Methodology (equal); Supervision (equal); Validation (equal); Writing – review & editing (equal). **Shao-Bin Qiu:** Conceptualization (equal); Methodology (equal). **Yao Yao:** Funding acquisition (equal); Project administration (equal); Supervision (equal); Writing – review & editing (equal).

DATA AVAILABILITY

The data that support the findings of this study are available within the article, its supplementary material, and the GitHub at https://github.com/Jia-Rui-Zeng/Orbital-Inversion (Ref. 43).

REFERENCES

[1]S. Gorgon, K. Lv, J. Grüne, B. H. Drummond, W. K. Myers, G. Londi, G. Ricci, D. Valverde, C. Tonnelé, P. Murto, A. S. Romanov, D. Casanova, V. Dyakonov, A. Sperlich, D. Beljonne, Y. Olivier, F. Li, R. H. Friend, and E. W. Evans, "Reversible spin-optical interface in luminescent organic radicals," Nature **620**, 538 (2023).
[2]H. Mao, G. J. Pazera, R. M. Young, M. D. Krzyaniak, and M. R. Wasielewski, "Quantum gate operations on a spectrally addressable photogenerated molecular electron spin-qubit pair," J. Am. Chem. Soc. **145**, 6585 (2023).
[3]H. Yu and T. Heine, "Magnetic coupling control in triangulene dimers," J. Am. Chem. Soc. **145**, 19303 (2023).
[4]A. Mizuno, R. Matsuoka, T. Mibu, and T. Kusamoto, "Luminescent radicals," Chem. Rev. **124**, 1034 (2024).
[5]Y.-J. Yu and F. Li, "Perspective on doublet electroluminescence from organic radicals," Appl. Phys. Lett. **126**, 100503 (2025).
[6]Q. Peng, A. Obolda, M. Zhang, and F. Li, "Organic light-emitting diodes using a neutral π radical as emitter: The emission from a doublet," Angew. Chem., Int. Ed. **54**, 7091 (2015).
[7]J. Zeng, S.-B. Qiu, Y.-J. Zhao, X.-B. Yang, and Y. Yao, "Quantum dynamics simulation of doublet excitation and magnetic field effect in neutral radical materials," J. Phys. Chem. Lett. **11**, 1194 (2020).
[8]G. Gryn'ova, M. L. Coote, and C. Corminboeuf, "Theory and practice of uncommon molecular electronic configurations," WIREs Comput. Mol. Sci. **5**, 440 (2015).
[9]Y. Wang, H. Zhang, M. Pink, A. Olankitwanit, S. Rajca, and A. Rajca, "Radical cation and neutral radical of Aza-thia[7]helicene with SOMO–HOMO energy level inversion," J. Am. Chem. Soc. **138**, 7298 (2016).
[10]H. Guo, Q. Peng, X.-K. Chen, Q. Gu, S. Dong, E. W. Evans, A. J. Gillett, X. Ai, M. Zhang, D. Credgington, V. Coropceanu, R. H. Friend, J.-L. Brédas, and F. Li, "High stability and luminescence efficiency in donor–acceptor neutral radicals not following the aufbau principle," Nat. Mater. **18**, 977 (2019).
[11]R. Murata, Z. Wang, Y. Miyazawa, I. Antol, S. Yamago, and M. Abe, "SOMO–HOMO conversion in triplet carbenes," Org. Lett. **23**, 4955 (2021).
[12]Y. Li, W.-K. Heng, B. S. Lee, N. Aratani, J. L. Zafra, N. Bao, R. Lee, Y. M. Sung, Z. Sun, K.-W. Huang, R. D. Webster, J. T. L. Navarrete, D. Kim, A. Osuka, J. Casado, J. Ding, and J. Wu, "Kinetically blocked stable heptazethrene and octazethrene: Closed-shell or open-shell in the ground state?" J. Am. Chem. Soc. **134**, 14913 (2012).
[13]S. S. SV, P. C. S. John, and R. S. Paton, "A quantitative metric for organic radical stability and persistence using thermodynamic and kinetic features," Chem. Sci. **12**, 13158 (2021).
[14]T. Sugawara and M. M. Matsushita, "Spintronics in organic π-electronic systems," J. Mater. Chem **19**, 1738 (2009).
[15]R. Zhao, K. Fu, Y. Fang, J. Zhou, and L. Shi, "Site-specific C(sp^3)–H aminations of imidates and amidines enabled by covalently tethered distonic radical anions," Angew. Chem., Int. Ed. **59**, 20682 (2020).
[16]E. Levernier, K. Jaouadi, H. Zhang, V. Corcé, A. Bernard, G. Gontard, C. Troufflard, L. Grimaud, E. Derat, C. Ollivier, and L. Fensterbank, "Phenyl silicates with substituted catecholate ligands: Synthesis, structural studies and reactivity," ChemEurJ **27**, 8782 (2021).
[17]L. Abella, J. Crassous, L. Favereau, and J. Autschbach, "Why is the energy of the singly occupied orbital in some radicals below the highest occupied orbital energy?" Chem. Mater. **33**, 3678 (2021).
[18]S. Kasemthaveechok, L. Abella, J. Crassous, J. Autschbach, and L. Favereau, "Organic radicals with inversion of SOMO and HOMO energies and potential applications in optoelectronics," Chem. Sci. **13**, 9833 (2022).
[19]S. Mishra, M. Vilas-Varela, S. Fatayer, F. Albrecht, D. Peña, and L. Gross, "Observation of SOMO-HOMO inversion in a neutral polycyclic conjugated hydrocarbon," ACS Nano **18**, 15898 (2024).
[20]Z. Li, X. Liu, Q. Bao, J. Wang, X. Liu, H. Gong, T. Han, C. Feng, D. Lu, L. Yue, C. Wu, G. He, and Y. Su, "The SUMO (singly unoccupied molecular orbital)-LUMO (lowest unoccupied molecular orbital) inversion radicals," J. Am. Chem. Soc. **147**, 1452 (2025).
[21]C.-C. He, S.-G. Xu, J. Zeng, W. Huang, Y. Yao, Y.-J. Zhao, H. Xu, and X.-B. Yang, "A graph-based statistical model for carbon nanostructures," J. Chem. Phys. **162**, 154104 (2025).
[22]C.-C. He, J. Zeng, Y.-J. Zhao, and X.-B. Yang, "A unified bonding entropy model to determine magnetic properties in graphene nanoflakes," arXiv:2505.09401 (2025).
[23]C. Bena and G. Montambaux, "Remarks on the tight-binding model of graphene," New J. Phys. **11**, 095003 (2009).
[24]S.-B. Qiu, Y.-J. Zhao, Y. Yao, and X.-B. Yang, "Possible high-spin states in hydrogenated C_{60} molecules," Phys. Rev. B **104**, 134409 (2021).
[25]B. Himmetoglu, A. Floris, S. De Gironcoli, and M. Cococcioni, "Hubbard-corrected DFT energy functionals: The LDA+U description of correlated systems," Int. J. Quantum Chem. **114**, 14 (2014).
[26]S. Dong, A. Obolda, Q. Peng, Y. Zhang, S. Marder, and F. Li, "Multicarbazolyl substituted TTM radicals: Red-shift of fluorescence emission with enhanced luminescence efficiency," Mater. Chem. Front. **1**, 2132 (2017).
[27]R. Pariser and R. G. Parr, "A semi-empirical theory of the electronic spectra and electronic structure of complex unsaturated molecules," I, J. Chem. Phys. **21**, 466 (1953).
[28]R. Pariser and R. G. Parr, "A semi-empirical theory of the electronic spectra and electronic structure of complex unsaturated molecules. II," J. Chem. Phys. **21**, 767 (1953).
[29]J. A. Pople, "Electron interaction in unsaturated hydrocarbons," Trans. Faraday Soc. **49**, 1375 (1953).
[30]M. Bedogni and F. Di Maiolo, "Singlet–triplet inversion in triangular boron carbon nitrides," J. Chem. Theory Comput. **20**, 8634 (2024).
[31]Q. Jiang, J. Zhang, Z. Mao, Y. Yao, D. Zhao, Y. Jia, D. Hu, and Y. Ma, "Room-temperature ferromagnetism in perylene diimide organic semiconductor," Adv. Mater. **34**, 2108103 (2022).
[32]J. Liu, J. Zeng, D. Zhao, Y. Yao, D. Hu, and Y. Ma, "Comprehending radicals, diradicals and their bondings in aggregates of imide-fused polycyclic aromatic hydrocarbons," Chem. Sci. **13**, 9985 (2022).
[33]X. He, D. Zhao, Y. Yao, J. Zhang, J. Zhou, X. Li, D. Hu, J. Yang, and Y. Ma, "Magnetic properties of self-assemble naphthalene diimide radical aggregates," Small **20**, 2311766 (2024).

[34]X. Li, Y.-L. Wang, C. Chen, Y.-Y. Ren, and Y.-F. Han, "A platform for blue-luminescent carbon-centered radicals," Nat. Commun. **13**, 5367 (2022).
[35]Z. Zhu, Z. Kuang, L. Shen, S. Wang, X. Ai, A. Abdurahman, and Q. Peng, "Dual channel emissions of Kasha and anti-Kasha from a single radical molecule," Angew. Chem., Int. Ed. **63**, e202410552 (2024).
[36]W.-P. Su, J. R. Schrieffer, and A. J. Heeger, "Solitons in polyacetylene," Phys. Rev. Lett. **42**, 1698 (1979).
[37]W. P. Su, J. R. Schrieffer, and A. J. Heeger, "Soliton excitations in polyacetylene," Phys. Rev. B **22**, 2099 (1980).
[38]J. Hubbard, "Electron correlations in narrow energy bands," Proc. R. Soc. London A **276**, 238 (1963).
[39]J. Hubbard, "Electron correlations in narrow energy bands. II. The degenerate band case," Proc. R. Soc. London A **277**, 237 (1964).
[40]J. Hubbard, "Electron correlations in narrow energy bands III. An improved solution," Proc. R. Soc. London A **281**, 401 (1964).
[41]A. Troisi and A. Shaw, "Very large π-conjugation despite strong nonplanarity: A path for designing new semiconducting polymers," J. Phys. Chem. Lett. **7**, 4689 (2016).
[42]H. Feldner, Z. Y. Meng, A. Honecker, D. Cabra, S. Wessel, and F. F. Assaad, "Magnetism of finite graphene samples: Mean-field theory compared with exact diagonalization and quantum Monte Carlo simulations," Phys. Rev. B **81**, 115416 (2010).
[43]J. Zeng (2025), "The orbital inversion program," GitHub. https://github.com/Jia-Rui-Zeng/Orbital-Inversion
[44]M. J. Frisch, G. W. Trucks, H. B. Schlegel, G. E. Scuseria, M. A. Robb, J. R. Cheeseman, G. Scalmani, V. Barone, G. A. Petersson, H. Nakatsuji, X. Li, M. Caricato, A. V. Marenich, J. Bloino, B. G. Janesko, R. Gomperts, B. Mennucci, H. P. Hratchian, J. V. Ortiz, A. F. Izmaylov, J. L. Sonnenberg, D. Williams-Young, F. Ding, F. Lipparini, F. Egidi, J. Goings, B. Peng, A. Petrone, T. Henderson, D. Ranasinghe, V. G. Zakrzewski, J. Gao, N. Rega, G. Zheng, W. Liang, M. Hada, M. Ehara, K. Toyota, R. Fukuda, J. Hasegawa, M. Ishida, T. Nakajima, Y. Honda, O. Kitao, H. Nakai, T. Vreven, K. Throssell, J. A. Montgomery, Jr., J. E. Peralta, F. Ogliaro, M. J. Bearpark, J. J. Heyd, E. N. Brothers, K. N. Kudin, V. N. Staroverov, T. A. Keith, R. Kobayashi, J. Normand, K. Raghavachari, A. P. Rendell, J. C. Burant, S. S. Iyengar, J. Tomasi, M. Cossi, J. M. Millam, M. Klene, C. Adamo, R. Cammi, J. W. Ochterski, R. L. Martin, K. Morokuma, O. Farkas, J. B. Foresman, and D. J. Fox, *Gaussian 16 Revision C.01* (Gaussian Inc., Wallingford, CT, 2016).
[45]A. D. Becke, "Density-functional thermochemistry. III. The role of exact exchange," J. Chem. Phys. **98**, 5648 (1993).
[46]C. Lee, W. Yang, and R. G. Parr, "Development of the Colle-Salvetti correlation-energy formula into a functional of the electron density," Phys. Rev. B **37**, 785 (1988).
[47]S. H. Vosko, L. Wilk, and M. Nusair, "Accurate spin-dependent electron liquid correlation energies for local spin density calculations: A critical analysis," Can. J. Phys. **58**, 1200 (1980).
[48]P. J. Stephens, F. J. Devlin, C. F. Chabalowski, and M. J. Frisch, "Ab initio calculation of vibrational absorption and circular dichroism spectra using density functional force fields," J. Phys. Chem. **98**, 11623 (1994).
[49]Y. Zhao and D. G. Truhlar, "The M06 suite of density functionals for main group thermochemistry, thermochemical kinetics, noncovalent interactions, excited states, and transition elements: Two new functionals and systematic testing of four M06-class functionals and 12 other functionals," Theor. Chem. Account. **120**, 215 (2008).
[50]J. Heyd, G. E. Scuseria, and M. Ernzerhof, "Hybrid functionals based on a screened Coulomb potential," J. Chem. Phys. **118**, 8207 (2003).
[51]T. Lu and F. Chen, "Multiwfn: A multifunctional wavefunction analyzer," J. Comput. Chem. **33**, 580 (2012).
[52]T. Lu, "A comprehensive electron wavefunction analysis toolbox for chemists, Multiwfn," J. Chem. Phys. **161**, 082503 (2024).
[53]W. Humphrey, A. Dalke, and K. Schulten, "VMD: Visual molecular dynamics," J. Mol. Graph. **14**, 33 (1996).